Bulletin of the Seismological Society of America, Vol. 87, No. 1, pp. 114–122, February 1997

Contribution of Seismic Tomography in Moment-Tensor Inversions Using Teleseismic Surface-Wave Spectra

by Hugues Dufumier and Jeannot Trampert

Abstract The knowledge of lateral heterogeneities is crucial for path corrections in moment tensor inversions using surface waves. After some attempts to use regionalized Earth models for very long-period surface-wave moment-tensor inversions, recent tomographic Earth models offer the possibility to make short-period path corrections and therefore retrieve more reliable moment tensors for teleseismic earthquakes. First we try to evaluate the precision required for path corrections in comparison with source effects. Some selected Earth models are tested to evaluate how their results compare to those using multiple-frequency filtering techniques. Some real cases illustrate the sensitivity of moment-tensor solutions to the different path corrections, and it appears clearly that regionalized Earth models and tomographic models deduced from long-period data alone (greater than 150 sec) cannot lead to trustworthy broadband moment-tensor inversions. Recent tomographic models using phase velocities at much shorter periods (40 to 200 sec) offer a precision comparable to that of the multiple-frequency filtering technique. Both methods lead to acceptable source mechanisms, using a small number of stations, in more than two cases out of three. The use of recent global tomographic models based upon shorter-period surface waves might thus be a useful alternative to heavy multiple-frequency filtering techniques to automate source studies, especially for rapid determinations using a small number of stations.

Introduction

The effect of lateral heterogeneities on surface-wave moment-tensor inversions is a well-known problem since the pioneer works of Patton (1980), Fitch *et al.* (1981), and Kanamori and Given (1981). The need to take into account large-scale heterogeneities in path corrections appeared even at very long periods. Nakanishi and Kanamori (1982) used the subdivision of the Earth in four zones of Dziewonski and Steim (1982) to perform Rayleigh-wave moment-tensor inversions in the period range 200 to 260 sec; Romanowicz and Monfret (1986) and Monfret and Romanowicz (1986) used the seven-zone regionalization of Okal (1977) for Rayleigh-wave moment-tensor inversions between 180 and 320 sec. Following Okal and Talandier (1989), Dufumier and Cara (1995) built a regionalized model comprising 10 zones on a 5° by 5° grid, based on ocean floor data (Nishimura and Forsyth, 1989) and Moho depths (Cadek and Martinec, 1991). They used this model for Love- and Rayleigh-wave spectra inversions for moment tensors between 35 and 350 sec.

Seismic tomography models seem the logical continuation of the above efforts, but so far they have hardly been used, mainly because of the lack of bandwidth of the data they are based upon. To retrieve source mechanisms from surface waves of teleseismic earthquakes (magnitude 5.5 to 7) and to constrain the inversions known for being ill-conditioned (Mendiguren, 1977; Kanamori and Given, 1981), it is indeed necessary to extend the bandwidth of the inverted spectra to shorter periods. This can be highlighted by looking at the variation of the condition number [ratio of the extreme singular values (Tarantola, 1987)] as a function of the frequency band used (Fig. 1): the wider the bandwidth, the lower the condition number. Since teleseismic moment-tensor inversions are usually unstable for condition numbers greater than 5 (Dufumier and Cara, 1995), it is necessary to use shorter periods to constrain moment-tensor inversions of superficial events or inversions with a limited station coverage. This can also be illustrated with the *a posteriori* data correlation matrix (Tarantola, 1987). It appears that it is necessary to use Rayleigh-wave spectra extending at least down to 50 sec or less to get data independent from the long-period ones (300 sec) (Fig. 2). For Love-wave data, the situation is worse as they are still strongly intercorrelated at all periods.

To perform moment-tensor inversions down to 30 or 40 sec, and lacking appropriate Earth models providing sufficiently accurate path corrections, attempts were made to extract the propagation from the data themselves with multiple-

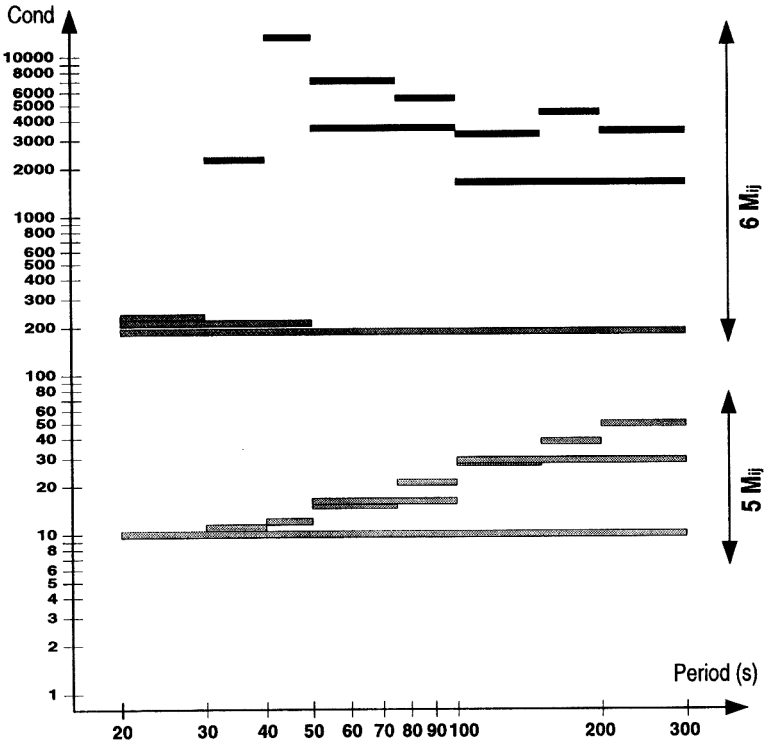

Figure 1. Variation of the condition number (Tarantola, 1987) of a moment-tensor inversion with the frequency band. In this case, we used two stations and a focal depth of 10 km with PREM (Dziewonski and Anderson, 1981). The value of the condition number is given on the vertical axis and coded by a gray scale, for different period bandwidths whose extension is shown horizontally. Values are given for full moment-tensor inversions and for deviatoric ones.

frequency filtering techniques (Jost and Herrmann, 1989; Jimenez *et al.*, 1989; Giardini *et al.*, 1994). Disadvantages are that lengthy processing needs to be applied to each signal, with constraints and results strongly depending on the noise level, and, in the absence of any knowledge of the source mechanism, the observed dispersion is an approximate one.

Since the 3D model *M*84 of Woodhouse and Dziewonski (1984), essentially based upon long-period surface waves, efforts have been made to increase lateral resolution (e.g., Zhang and Tanimoto, 1993) and vertical resolution (e.g., Su *et al.*, 1994). A new generation of models (Ekström and Dziewonski, 1995; Woodhouse and Trampert, 1995a, 1995b), based upon short-period phase velocity maps derived from tens of thousands of measurements and many body waveforms, have unprecedented lateral and vertical resolution over the whole globe and show new features in the uppermost mantle. Even if the discrepancies of path corrections obtained from different tomographic models are still high compared to the precision required for source studies, they present a clear improvement over regionalizations. They might even offer an interesting alternative to multiple-frequency filtering techniques in the near future, opening the possibility to completely automate rapid determinations of source parameters.

The main goal of this article is to compare different path corrections for moment-tensor inversions and to show that tomographic models based upon short-period surface waves give results at least comparable to those of multiple-frequency filtering techniques. In this study, we concentrate on linear moment-tensor inversions of surface waves observed at a few stations only: This configuration is particularly useful for rapid determinations of preliminary mechanisms within an hour of the event. Our intention here is not to obtain final and detailed mechanisms. We refer to the article of Dufumier and Cara (1995) for the methodological description. We will focus our attention on the effects of various path corrections using a given technique. At the end, we will present a comparison of our results with a similar, routinely used, technique, the centroid moment-tensor (CMT) inversion (Dziewonski *et al.*, 1981), which, using many more stations and different waves, is quite acceptable on average.

Source and Path Effects

Linear surface-wave moment-tensor inversions are performed using real and imaginary parts of surface-wave spectra, the real part giving the vertical dip-slip component of the source, the imaginary part the 45° dip-slip, strike-slip, and isotropic components (Dufumier, 1995). The phase of the data, which depends on the source mechanism, the source history, and the phase velocity along the path, is very convenient for different comparisons. The amplitudes are mostly dependent on the radiation of the mechanism and to a lesser extent on focusing effects (e.g., Woodhouse and Wong, 1986) and on the lateral variations in attenuation (Tsai and Aki, 1969; Levshin, 1985). We will not consider the two latter effects in this article, which are still imperfectly modeled at a global scale to date.

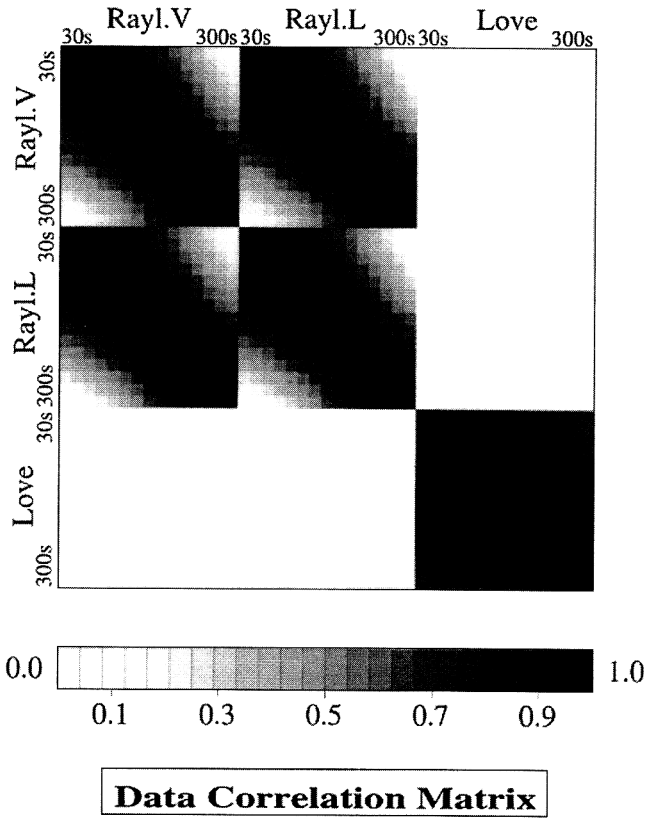

Figure 2. The *a posteriori* correlation matrix in the data space for the inversion of three-component single-station radiation spectra. The correlation coefficient is normalized and may vary from −1 to 1: In the present case, there are no negative correlations, 0 indicates independent data, and 1 indicates fully correlated data. Short-period (30 to 50 sec) and long-period (300 sec) Rayleigh data appear to carry independent information. For Love waves, short and long periods are still correlated at 60%.

The influence of some path effects on linear moment-tensor inversions has been studied by Patton and Aki (1979), together with the question of the simultaneous resolution of source and path effects (Patton, 1980). As an illustration, we compare in Figure 3 typical frequency variations of the different terms constitutive of the phase of surface-wave spectra: the phase associated with the radiation of the source, the linear phase dependence of a triangular source-time function, and the phase lag due to an error in phase velocity along the path. A shift in origin time or a source mislocation are equivalent to the effect of source duration. To limit interferences with the phase of the source mechanisms, it is necessary to estimate the source duration with a precision of a few seconds.

In absence of any knowledge of the source mechanism, the radiation phase is usually supposed to be almost flat between 30 and 300 sec of period, in comparison to the other effects. In fact, it may present a sharp local jump that may reach 180° (Fitch *et al.*, 1981; Dufumier, 1995) and depends on the source depth and on the position of the station relatively to the nodal planes (Fig. 3). The assumption of a zero group delay at the source, which is used in multiple-frequency filtering techniques when the mechanism is unknown (Jimenez *et al.*, 1989), is thus acceptable except in local parts of the frequency band.

Phase errors due to lateral heterogeneities are much larger than the previous effects, making the retrieval of the source phases almost impossible. A reasonable error of 1% on phase velocities results in phase deviations of some tens of degrees at periods greater than 100 sec and of hundreds of degrees at short periods.

An example of phase velocity determinations for different Earth models is shown in Figure 4. The corresponding phase errors are also shown, as well as a comparison to the source phases. The measurement of phase velocity using the multiple-frequency filtering technique (Jimenez *et al.*, 1989), including corrections for the mechanism and for source duration, serves as a reference. It can be seen that most models present strong deviations to the observed dispersion. On the other hand, a recent phase velocity model such as that of Trampert and Woodhouse (1996), referred to hereinafter as TW96, presents a reasonable fit over the whole bandwidth. Note that the path presented here was not used in the construction of the TW96 maps.

Comparisons of Path Corrections

We selected 100 Love and Rayleigh ray paths to analyze the statistics of phase velocity deviations for different Earth models (Fig. 5). Earthquakes were chosen with an approximate magnitude of 6.5, in order to combine a clear multiple-frequency filtering technique picking up to 300 sec and source durations lower than the shortest periods used (35 sec). We ensured a good variety of source mechanisms and of source media, as well as a homogeneous distribution of paths.

In Figure 6, we represent the averaged relative errors of phase velocities, for three Earth models: PREM (Dziewonski and Anderson, 1981), *M*84 (Woodhouse and Dziewonski, 1984), and the phase velocity model TW96. We neglected regionalized models, as they give far worse results. We compute two different errors relative to measurements using the multiple-frequency filtering technique, that serves as reference observation, for three period ranges, 35 to 60, 60 to 100, and 100 to 200 sec:

- the average phase velocity deviation from the observed one: $\Sigma(C - C_{obs})/\Sigma C_{obs}$
- the relative standard deviation: $\Sigma|C - C_{obs}|/\Sigma C_{obs}$

The error histograms are presented for the whole data set and for subgroups: short paths (2500 to 6000 km), medium paths (6,000 to 12,000 km), and long paths (more than 12,000 km), pure oceanic or pure continental paths, partic-

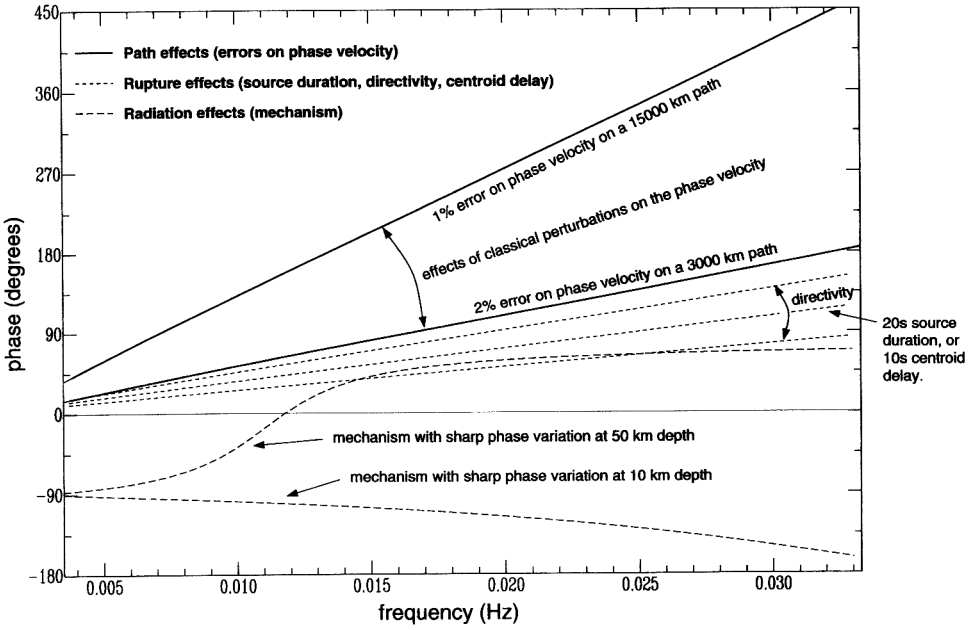

Figure 3. Phase variations in degrees for different terms affecting the phase of surface waves between 35 and 300 sec: maximum variations of radiation phases for mechanisms with rapid phase variations, at 10 and 50 km in depth; linear phase variation due to a triangular source-time function of 20 sec in duration, equivalent to the phase lag due to an error of 10 sec on the origin time; and phase errors due to standard phase velocity errors, on short and long paths. While errors in the source duration and phase velocity do not affect the long-period end of the radiation phase very much, keeping information on the mechanism at short periods implies a precision of a few seconds on the source duration, of 1% on short path phase velocities, and of less than 0.3% on long path phase velocities.

ular paths (along trenches or mountain belts), and mixed paths.

Although it is a continuous tomographic model, the model *M*84 represents only a slight improvement compared to PREM. Both models are good at long periods, but *M*84, deduced from long-period data, is not really appropriate for short-period studies. The main improvements concern short and particular paths, where heterogeneities are the most sensitive.

The phase velocity model TW96 shows a clear improvement for the determination of phase velocities compared to the two latter models, both in average and standard deviations. Standard errors are below the critical 1% level, even at short periods. As any model, it is of course less precise for short paths, continental and particular paths, especially for Love waves. But we observe very good results for medium and mixed paths.

Numerically speaking, average standard errors on phase velocities, considering the whole frequency bandwidth (35 to 200 sec), are of 1.45% for PREM, 1.1% for *M*84, and 0.64% for TW96. In terms of phases, this leads to phase variations in the frequency band 35 to 200 sec of 490°, 350°, and 175°, respectively. The latter is comparable to the maximum expectable phase variation due to source mechanisms. Therefore, standard phase errors generated by the phase velocity model TW96 are of the same order as the maximum errors imputable to the multiple-frequency filtering technique. Note that about 60% of the paths used in this study were also used in the construction of TW96, a proportion that reflects the high path density of the TW96 model.

Moment-Tensor Inversions

One can easily imagine that if phase errors due to inappropriate path corrections are much larger than the radiation phases, data are sufficiently perturbed to lead to moment-tensor solutions with a low confidence level. Particularly, the ratio between the vertical dip-slip and the other components of the moment tensor is then unconstrained, leading to erroneous mechanisms.

After the problem of the accuracy of the different path corrections, the final question is to see if high-resolution phase velocity models and the multiple-frequency filtering technique retrieve acceptable source mechanisms in simple configurations.

Of course, the solution of moment-tensor inversions does not only depend on path corrections but also on the number of stations, and even more so on the distribution of stations. Therefore, in order to eliminate most instabilities due to the number of stations, we have performed inversions

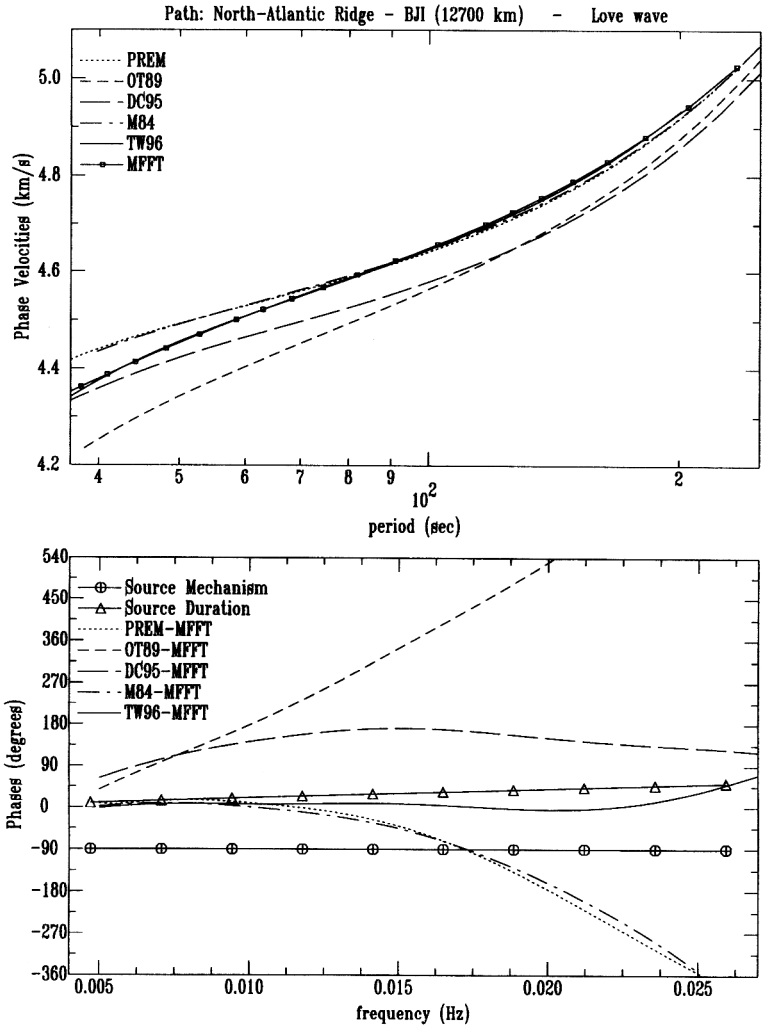

Figure 4. Typical variations in phase velocities (top) and corresponding phase errors (bottom) for different path corrections: using PREM (Dziewonski and Anderson, 1981) (dotted lines), the regionalized model of Okal and Talandier (1989) (short-dashed lines), the regionalized model of Dufumier and Cara (1995) (long-dashed lines), *M*84 (Woodhouse and Dziewonski, 1984) (short- and long-dashed lines), TW96 (Trampert and Woodhouse, 1996) (solid lines), and the multiple-frequency filtering technique (MFFT) for group velocity picking (solid lines with symbols). The period ranges from 38 to 250 sec. Source phases (radiation of the mechanism and source history) are added for comparison. The path used in this example is shown bold in Figure 5.

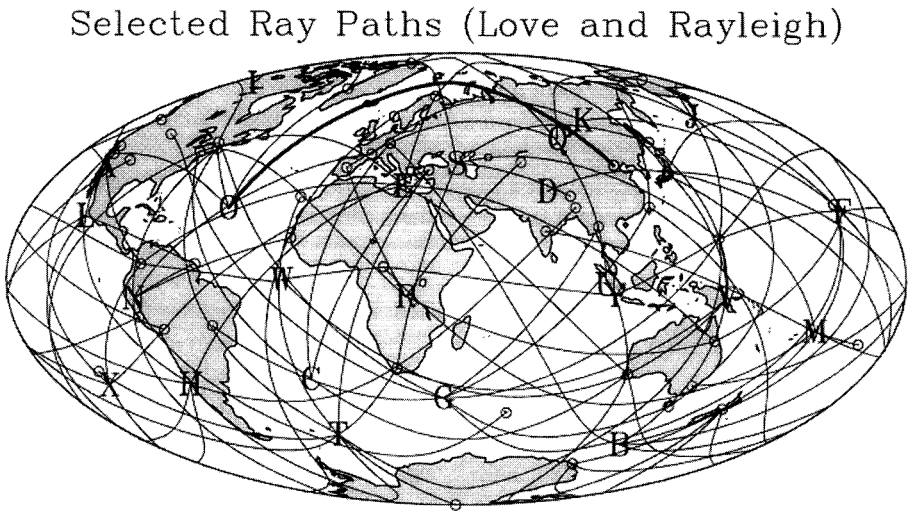

Figure 5. 100 surface-wave ray paths used in this study to compute mean phase velocities along the minor arcs using different Earth models. The equal-area Mollweide projection is centered at 45° E and the equator. The letters indicate the different epicenters, and the circles, seismic stations. The bold line refers to the path used in Figure 4.

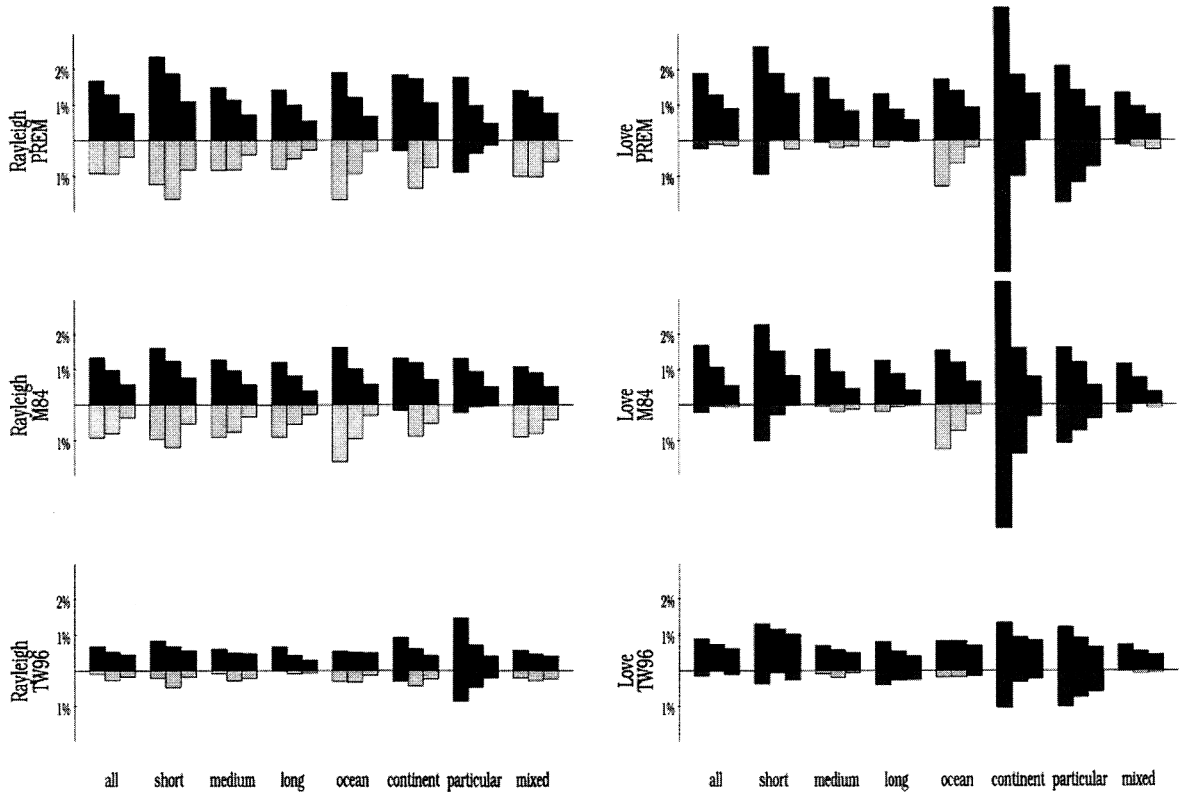

Figure 6. Histograms of relative errors of phase velocities for different models relative to measurements from the multiple-frequency filtering technique, averaged over all the paths, or over subgroups: short paths (2500 to 6000 km), medium paths (6,000 to 12,000 km), long paths (more than 12,000 km), pure oceanic or pure continental paths, particular paths (along trenches or mountain belts), and mixed paths. The upper black box indicates the standard deviation, and the lower box, the average deviation, in light gray for negative values and dark gray for positive values. The three boxes of each histogram correspond from left to right to the period ranges 35 to 60, 60 to 100,

for all earthquakes of Figure 5 for which more than five three-component stations were available, with a good signal-to-noise ratio. The isotropic component of the source has been fixed to be zero, since inversions for full moment tensor are usually unstable (Dufumier and Cara, 1995). Earthquake depths range from 10 to 85 km, and some unavoidable instabilities might still occur for the shallowest. We therefore eliminated solutions for which both the condition number and the resolution matrix (Tarantola, 1987) indicated potentially unstable results.

Classically, inversions were performed iteratively on a set of depths and source durations (Romanowicz, 1982; Romanowicz and Monfret, 1986). On these grids, the mechanisms, obtained from surface waves only, appear to be relatively stable, even if the depth and source duration would be better constrained using shorter-period body waves (Ekström, 1989; Dufumier and Cara, 1995; Dufumier, 1996). The best solution is considered as the one corresponding to the minimum cost function (Tarantola, 1987).

Results are shown in Figure 7 for a visual estimation of the quality of the retrieved source mechanism. We present the CMT (Dziewonski *et al.*, 1981) solution as one of the possible references, in order to propose a comparison with homogeneous results of a similar, routinely used method, whose main advantage over ours is that it uses many more surface-wave records and also body waves. Since some CMT mechanisms might differ significantly from other published solutions (e.g., Chung and Brantley, 1989), we checked that those of Figure 7 are in good agreement with the mechanisms obtained from polarities and with the moment-tensor solution published by the NEIC, when available.

An acceptable mechanism was retrieved three times out of nine using PREM (Dziewonski and Anderson, 1981), four times out of nine using the regionalized model (Dufumier and Cara, 1995), five times out of nine using *M*84 (Woodhouse and Dziewonski, 1984), and seven times out of nine using TW96 (Trampert and Woodhouse, 1996) or the multiple-frequency filtering technique.

The same evolution may be observed on the seismic moment (Table 1). This reflects the observable trade-off between the seismic moment and lateral heterogeneities (Patton and Aki, 1979; Ekström, 1989). The fact that the re-

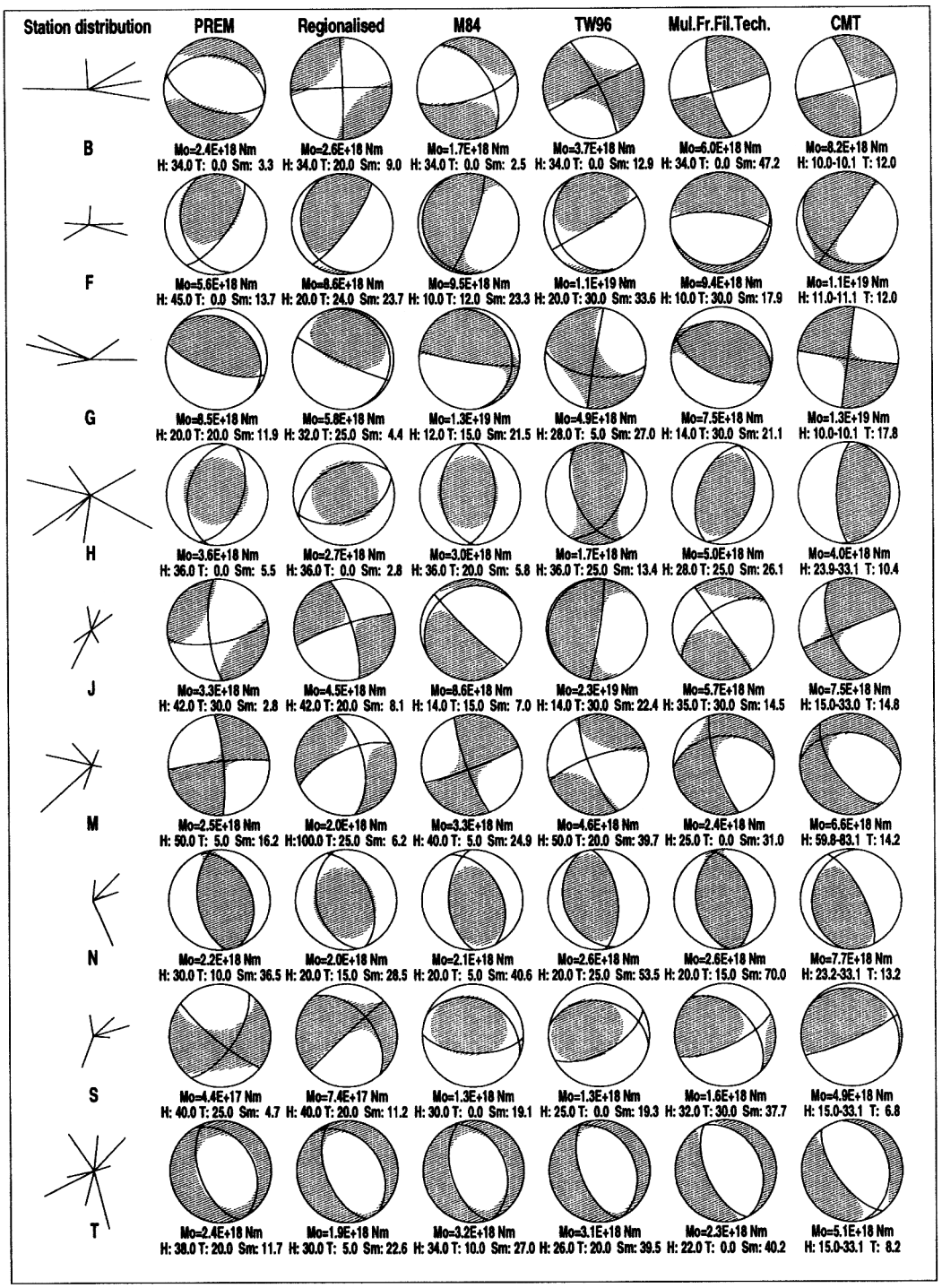

Figure 7. Moment-tensor inversions for nine earthquakes used in Figure 5 for which more than five three-component stations were available with good signal-to-noise ratio. The station distribution, in azimuth and distance, is symbolized on the left (distances range from 3,000 to 17,000 km). The letters refer to the epicenters in Figure 5. Preinversion path corrections were performed using (from left to right) PREM (Dziewonski and Anderson, 1981), regionalized Earth model (Dufumier and Cara, 1995), *M*84 (Woodhouse and Dziewonski, 1984), phase velocity models (Trampert and Woodhouse, 1996), and the multiple-frequency filtering technique. For each inversion are indicated the deviatoric moment tensor, the best double-couple, the seismic moment M_0, the best depth H (km), the best source duration T (sec), and the best cost function reduction S_m (in %). The last column indicates, as one possible reference, the final CMT solution, including the centroid depth and the NEIC depth.

Table 1

Average values of the ratio $M_0/M_{0\text{CMT}}$ for each of the models used in Figure 7; of the best rms fit to the data; and of the best cost function reduction S_m (in %).

	PREM	Regionalized Dufumier 95	M84	TW96	Multiple-Freq. Filtering Tech.
Ratio $M_0/M_{0\text{CMT}}$	0.38	0.39	0.53	0.59	0.63
rms	0.96	0.99	0.94	0.92	0.88
Cost function (%)	11.8	12.9	19.1	29.0	34.0

trieved seismic moment is systematically lower than the CMT one is partially due to damping in the inversion, and to the fact that no body waves were used here.

The evolution of the root mean square (rms) fit and of the cost function as a function of the type of path correction used are even clearer (Table 1). The rms, measuring the fit of the data, is more sensitive to their amplitudes than to their phases and therefore varies slowly. However, the cost function, which is the quantity minimized in the inversion process, shows clearly that it is much easier to retrieve a model explaining physically plausible phases than abnormal ones.

Conclusions

To retrieve uncontaminated source phases from path effects, techniques of extraction of the surface-wave dispersion, either from Earth models or from the data themselves, require a very high precision: The relative error on phase velocities along standard paths should not exceed 0.5%, even at short periods. The bandwidth used for the inversion should be as broad as possible for better conditioning but should be restricted when such a precision on phase velocities is not available or when the signal-to-noise ratio is poor.

The multiple-frequency filtering technique, although based on the approximation of a zero group delay at the source, still gives the best path corrections when data are sufficiently clean to ensure clear dispersion picking. The technique, however, has limitations, at short and very long periods, and at short and antipodal distances. And it implies, most of the time, decisional human interaction.

A new generation of high-resolution (lateral and vertical) tomographic models based upon short-period phase velocity measurements presents an interesting alternative for the future of teleseismic moment-tensor inversions. Even if such models already lead to acceptable results in more than two cases out of three, they still require short scale refinements, especially in continental and particular zones, to be precise enough for source studies. Adding other finely gridded geophysical data, such as the model 3SMAC of Nataf and Ricard (1996), might improve source determinations further. The advantage of tomographic models over interactive measurements is that they permit the full automatization of surface-wave moment-tensor inversions, even in the case of noisy records. They may at least provide a useful starting base for automated picking of dispersion curves. This automatization is most interesting for rapid determination of preliminary mechanisms (within an hour following the event) using a small number of stations.

Of course, when regional tomographic models are available with high confidence levels at even shorter periods, the same conclusions are applicable to regional moment-tensor inversions, using wavelengths in agreement with the lateral resolution of the models (Romanowicz *et al.*, 1993).

Acknowledgments

During the course of this work, H. Dufumier benefited from a BDI-Ph.D. Grant from CNRS. Work was performed at URA 1358 of CNRS, Laboratoire de Sismologie of Université Louis Pasteur, Strasbourg. We used IRIS/DMC and Géoscope data. We thank Barbara Romanowicz for a constructive review.

References

Cadek, O. and Z. Martinec (1991). Spherical harmonic expansion of the Earth's crustal thickness up to degree and order 30, *Studia Geophys. Geod.* **35,** 151–165.

Chung, W.-Y. and B. J. Brantley (1989). The 1984 southern Yellow Sea earthquake of eastern China: source properties and seismotectonic implications for a stable continental area, *Bull. Seism. Soc. Am.* **79,** 1863–1882.

Dufumier, H. (1995). Détermination de Tenseurs des Moments Sismiques à partir d'Ondes de Volume et de Surface Télésismiques—Approches Directes et Inverses, Limites d'Applicabilité, *Ph.D. Thesis*, EOPGS, Université Louis Pasteur, Strasbourg.

Dufumier, H. and M. Cara (1995). On the limits of linear moment tensor inversion of surface wave spectra, *Pageoph* **145,** 235–257.

Dufumier, H. (1996). On the limits of linear moment tensor inversion of teleseismic body wave spectra, *Pageoph.* **147,** 467–482.

Dziewonski, A. M. and D. L. Anderson (1981). Preliminary reference Earth model, *Phys. Earth Planet. Interiors* **25,** 297–356.

Dziewonski, A. M., T. A. Chou, and J. H. Woodhouse (1981). Determination of earthquake source parameters from waveform data for studies of global and regional seismicity, *J. Geophys. Res.* **86,** 2825–2852.

Dziewonski, A. M. and J. M. Steim (1982). Dispersion and attenuation of mantle waves through waveform inversion, *Geophys. J. R. Astr. Soc.* **70,** 503–527.

Ekström, G. (1989). A very broad band inversion method for the recovery of earthquake source parameters, *Tectonophysics*, **166,** 73–100.

Ekström, G. and A. M. Dziewonski (1995). Improved models of upper mantle S velocity structure (abstract supplement), *EOS* **76,** no. 46, 421.

Fitch, T. J., R. G. North, and M. W. Shields (1981). Focal depths and moment tensor representations of shallow earthquakes associated with the Great Sumba earthquake, *J. Geophys. Res.* **86,** 9357–9374.

Giardini, D., L. Malagnini, B. Palombo, and E. Boschi (1994). Broad-band moment tensor inversion from single station, regional surface waves for the 1990, N.W.-Iran earthquake sequence, *Ann. Geofis.* XXXVII, no. 6, 1645–1657.

Jimenez, E., M. Cara, and D. Rouland (1989). Focal mechanisms of moderate-size earthquakes from the analysis of single-station three component surface wave records, *Bull. Seism. Soc. Am.* **79,** 955–972.

Jost, M. L. and R. B. Herrmann (1989). A student's guide to and review of moment tensors, *Seism. Res. Lett.* **60,** 37–57.

Kanamori, H. and J. W. Given (1981). Use of long-period surface waves for rapid determination of earthquake source parameters, *Phys. Earth Planet. Interiors* **27,** 8–31.

Levshin, A. L. (1985). Effects of lateral inhomogeneities on surface wave amplitude measurements, *Ann. Geophys.* **3,** no. 4, 511–518.

Mendiguren, J. A. (1977). Inversion of surface wave data in source mechanism studies, *J. Geophys. Res.* **82,** no. 5, 889–894.

Monfret, T. and B. Romanowicz (1986). Importance of on scale observations of first arriving rayleigh wave trains for source studies: example of the Chilean event of March 3, 1985, observed on the géoscope and IDA networks, *Geophys. Res. Lett.* **13,** no. 10, 1015–1018.

Nakanishi, I. and H. Kanamori (1982). Effects of lateral heterogeneity and source process time on the linear moment tensor inversion of long-period Rayleigh waves, *Bull. Seism. Soc. Am.* **72,** 2063–2080.

Nataf, H. C. and Y. Ricard (1996). 3SMAC: an a priori tomographic model of the upper mantle based on geophysical modelling, *Phys. Earth Planet. Interiors,* **95,** 101–122.

Nishimura, C. E. and D. W. Forsyth (1989). The anisotropic structure of the upper mantle in the Pacific, *Geophys. J.* **96,** 203–229.

Okal, E. A. (1977). The effect of intrinsic ocean upper mantle heterogeneity on the regionalisation of long period Rayleigh wave phase velocities, *Geophys. J. R. Astr. Soc.* **49,** 357–370.

Okal, E. A. and J. Talandier (1989). M_m: a variable-period mantle magnitude, *J. Geophys. Res.* **94,** no. B4, 4169–4193.

Patton, H. and K. Aki (1979). Bias in the estimate of seismic moment tensor by the linear inversion method, *Geophys. J. R. Astr. Soc.* **59,** 479–495.

Patton, H. (1980). Reference point equalization method for determining the source and path effects of surface waves, *J. Geophys. Res.* **85,** no. B2, 821–848.

Romanowicz, B. (1982). Lateral heterogeneity in continents: moment tensor inversion of long-period surface waves and depth resolution of crustal events; body-wave modelling and phase-velocity calibrations, *Phys. Earth Planet. Interiors* **30,** 269–271.

Romanowicz, B. and T. Monfret (1986). Source process times and depths of large earthquakes by moment tensor inversion of mantle wave data and the effect of lateral heterogeneity, *Ann. Geophys.* **4,** 271–283.

Romanowicz, B., D. S. Dreger, M. Pasyanos *et al.* (1993). Mode of strain release in central and northern California, *Geophys. Res. Lett.* **20,** 1643–1646.

Su, W., R. L. Woodward, and A. M. Dziewonski (1994). Degree 12 model of shear velocity heterogeneity in the mantle, *J. Geophys. Res.* **99,** 6945–6980.

Trampert, J. and J. H. Woodhouse (1996). High resolution global phase velocity distributions, *Geophys. Res. Lett.* **23,** 21–24.

Tarantola, A. (1987). *Inverse Problem Theory, Methods for Data Fitting and Model Parameter Estimation,* Elsevier, Amsterdam.

Tsai, Y. B. and K. Aki (1969). Simultaneous determination of the seismic moment and attenuation of seismic surface waves, *Bull. Seism. Soc. Am.* **59,** 275–287.

Woodhouse, J. H. and A. M. Dziewonski (1984). Mapping the upper mantle: three dimensional modelling of Earth structure by inversion of seismic waveforms, *J. Geophys. Res.* **89,** 5953–5986.

Woodhouse, J. H. and J. Trampert (1995a). Global Crustal and Mantle Structure Inferred from Surface Wave and Other Data, IUGG XXI General Assembly, Boulder.

Woodhouse, J. H. and J. Trampert (1995b). Global upper mantle structure inferred from surface wave and body wave data (abstract supplement), *EOS,* **76,** 422.

Woodhouse, J. H. and Y. K. Wong (1986). Amplitude, phase and path anomalies of mantle waves, *Geophys. J. R. Astr. Soc.* **87,** 753–774.

Zhang, Y.-S. and Tanimoto, T. (1993). High-resolution global upper mantle structure and plate tectonics, *J. Geophys. Res.* **98,** 9793–9823.

Institut de Physique du Globe
5 rue Descartes
67084 Strasbourg cedex, France
(H.D., J.T.)

Dipartimento di Scienze della Terra,
Via Weiss 1
34127 Trieste, Italia
(H.D.)

Department of Geophysics
University of Utrecht
P.O. Box 80021
3508 TA Utrecht
The Netherlands
(J.T.)

Manuscript received 24 October 1995.